One-Stop-Shop Whole-Body ^{68}Ga-PSMA-11 PET/MRI Compared with Clinical Nomograms for Preoperative T and N Staging of High-Risk Prostate Cancer

Mark Thalgott[1], Charlotte Düwel[1], Isabel Rauscher[2], Matthias M. Heck[1], Bernhard Haller[3], Andrei Gafita[2], Jürgen E. Gschwend[1], Markus Schwaiger[2], Tobias Maurer[1], and Matthias Eiber[2,4]

[1]Department of Urology, Klinikum Rechts der Isar, Technical University of Munich, Munich, Germany; [2]Department of Nuclear Medicine, Klinikum Rechts der Isar, Technical University of Munich, Munich, Germany; [3]Institute of Medical Statistics and Epidemiology, Klinikum Rechts der Isar, Technical University of Munich, Munich, Germany; and [4]Department of Molecular and Medical Pharmacology, David Geffen School of Medicine at UCLA, Los Angeles

Our aim was to assess the diagnostic potential of 1-stop-shop prostate-specific membrane antigen ligand (^{68}Ga-PSMA-11) PET/MRI compared with preoperative staging nomograms in patients with high-risk prostate cancer. **Methods:** A total of 102 patients underwent ^{68}Ga-PSMA-11 PET/MRI before intended radical prostatectomy with lymph node dissection. Preoperative variables determined the probabilities for lymph node metastases (LNM), extracapsular extension (ECE), and seminal vesical involvement (SVI) using the Memorial Sloan Kettering Cancer Center (MSKCC) nomogram and Partin tables. Receiver-operating-characteristic analyses were performed to determine best discriminatory cutoffs. On a cohort basis, positivity rates of imaging and nomograms were compared with pathologic prevalence. On a patient basis, sensitivity, specificity, and area under the curves were calculated. Finally, the full concordance of each method to postoperative T and N stage was determined. **Results:** Seventy-three patients were finally analyzed. On a cohort basis, the MSKCC nomogram (39.7%) positivity rate was most concordant with pathologic prevalence for LNM (34.3%) compared with Partin tables (14.1%) and imaging (20.6%). Prevalence of ECE (72.6%) was best predicted by MSKCC nomograms and imaging (83.6% each), compared with Partin tables (38.4%). For prevalence of SVI (45.2%), imaging (47.9%) performed superior to MSKCC (37.6%) and Partin tables (19.3%). On a patient basis, AUCs for LNM, ECE, and SVI did not differ significantly between tests ($P > 0.05$). Imaging revealed a high specificity (100%) for LNM and a sensitivity (60%) comparable to the MSKCC nomogram (68%) and Partin tables (60%). For ECE, imaging revealed the highest sensitivity (94.3%) compared with the MSKCC nomogram (66%) and Partin tables (71.1%). For SVI, sensitivity and specificity of imaging and the MSKCC nomogram were comparable (81.5% and 80% vs. 87.9% and 75%). The rate of concordance to the final pTN stage was 60.3% for imaging, 52.1% for the MSKCC nomogram, and 39.7% for Partin tables. **Conclusion:** In our analysis, preoperative 1-stop-shop ^{68}Ga-PSMA-11 PET/MRI performs at least equally for T and N stage prediction compared with nomograms in high-risk prostate cancer patients. Despite an improved prediction of the full final stage and the yield of additional anatomic information, the use of ^{68}Ga-PSMA-11 PET/MRI warrants further prospective evaluation.

Received Jan. 2, 2018; revision accepted Apr. 23, 2018.
For correspondence or reprints contact: Mark Thalgott, Department of Urology, Klinikum Rechts der Isar, Technical University of Munich, Ismaninger Strasse 22, 81675 Munich, Germany.
E-mail: m.thalgott@web.de
Guest Editor: Ken Herrmann, University Hospital Essen
Published online May 24, 2018.

Key Words: prostate-specific membrane antigen; prostate cancer; Partin tables; staging nomogram; ^{68}Ga-PSMA-11 PET/MRI

J Nucl Med 2018; 59:1850–1856
DOI: 10.2967/jnumed.117.207696

Accurate primary staging in patients with prostate cancer (PC) is crucial for planning individualized treatment strategies especially before radical prostatectomy (RP) in conjunction with pelvic lymph node dissection (*1,2*). Patients with high-risk classification are prone to harbor locally advanced disease with extracapsular extension (ECE), seminal vesicle extension (SVI), or lymph node metastases (LNM) (*3*).

Therefore, staging nomograms are often used by urologists to predict the risk of advanced disease. Commonly these nomograms use the prostate-specific antigen (PSA) value at diagnosis, biopsy Gleason score, and local clinical stage as assessed by digital rectal examination (*4–6*). Nevertheless, nomograms provide an estimate of probability but do not offer individualized binary results indicating the presence or absence of disease (*7*). Moreover, they do not incorporate anatomic data that could guide treatment (*8*).

Routine staging using CT or MRI lacks sufficient accuracy especially for detection of subcentimeter LNM (*9*). PET combined with cross-sectional imaging (CT or MRI) can potentially overcome limitations of morphologically based imaging. Until recently, ^{18}F-fluorocholine or ^{11}C-choline have been used but still resulted in a low sensitivity, for example, for LNM detection (*7,10,11*). During the last years, considerable advances for PC local and distant staging have been reported using probes targeting the prostate-specific membrane antigen (PSMA) in newly diagnosed and recurrent PC (*12–17*). Simultaneous ^{68}Ga-PSMA-11 PET/MRI improves diagnostic accuracy for cancer (PC) localization in the prostate when compared with multiparametric MRI (*12*). Similarly, lymph node staging with ^{68}Ga-PSMA-11 PET proved to be superior to standard routine cross-sectional imaging (*13,16*). Consequently, a combination of PET and MRI exploiting both the superb molecular information from ^{68}Ga-PSMA-11 PET and the high local contrast of MRI for whole-body primary staging is expected to increase prediction of local, nodal and distant tumor burden.

Therefore, the main objective of our study was to compare the performance of a preoperative 1-stop-shop ^{68}Ga-PSMA-11 PET/MRI with clinical staging nomograms for T and N staging in patients with high-risk PC validated by histopathology.

MATERIALS AND METHODS

Patients

A retrospective database search of all PC patients having undergone ^{68}Ga-PSMA-11 PET/MRI between December 2012 and November 2015 has been conducted. Criteria for inclusion of patients in this analysis were as follows: histologically proven (D'Amico criteria) high-risk PC and eligibility to perform RP on the basis of clinical assessment of the patient (e.g., history, physical examination) by an experienced urologist. All patients gave written informed consent for the imaging study and RP. This retrospective study was approved by the ethics committee of the Klinikum Rechts der Isar, Technical University of Munich, Munich, Germany (permit 5665/13) and was performed according to the ethical standards of the Declaration of Helsinki as well as national regulations.

^{68}Ga-PSMA-11 PET/MRI

Patients received an intravenous injection of ^{68}Ga-PSMA-11 (median, 138 MBq; interquartile range [IQR], 114–156) synthesized as described previously (*18*). Imaging was performed with a median interval of 55 min after injection (IQR, 50–67) using an integrated whole-body PET/MRI system (Siemens Biograph mMR; Siemens Healthcare). Whole-body coronal T1 turbo spin echo and axial T2 haste sequences and simultaneous PET with 5 min per bed position were acquired. Multiparametric MRI of the prostate was performed in parallel to a 15-min PET acquisition as described in Supplemental Table 1 (supplemental materials are available at http://jnm.snmjournals.org). To reduce artifacts due to high tracer activity in the urinary system, all patients received coinjection of furosemide and were asked to void urine directly before the start of the examination.

Image Analysis

A double-trained board-certified radiologist and nuclear medicine physician (with 10 y of experience) reviewed the imaging datasets masked to postoperative clinical and pathologic data. ^{68}Ga-PSMA-11 PET/MR images were evaluated using commercial image viewing software for multiparametric MRI (Easy Vision; Philips) and PET (Syngo TrueD; Siemens Medical Solutions). Local T staging was evaluated according to the American Joint Committee on Cancer. For N staging, a 3-point Likert scale with the following categories was used: 1 = LNM present; 2 = equivocal/intermediate; 3 = no LNM (*19*). The diagnosis of LNM was based on 1 = LNM present: suspicious focal increased ^{68}Ga-PSMA-11 uptake (higher than liver) corresponding to a lymph node independent of the short-axis diameter or short-axis diameter > 10 mm; 2 = equivocal/intermediate: ^{68}Ga-PSMA-11 uptake clearly higher than background in vessels, but not higher than liver or round configuration with a short-axis diameter 8–10 mm; and 3 = no LNM: no ^{68}Ga-PSMA-11 uptake or as faint as background or short-axis diameter < 8 mm. Finally, for M staging the presence and location of lesions suggestive of distant metastases were noted. For example, for bone metastases the following criteria were used: 1 = bone metastases present: suspicious focal increased ^{68}Ga-PSMA-11 uptake (higher than liver) or unanimously hypointense lesion on T1-weighted not representing a bone island or degenerative changes; 2 = equivocal/intermediate: ^{68}Ga-PSMA-11 uptake clearly higher than background in vessels, but not higher than liver or unclear T1-weighted hypointensity; and 3 = no bone metastases: no ^{68}Ga-PSMA-11 uptake or as faint as background or unsuspicious bone marrow signal on T1-weighted.

Imaging criteria for the presence of SVI included the lack of architecture of the seminal vesicle, areas of hypointense T2-weighted (T2w) signal intensity, direct extension of a T2w hypointense tumor into the seminal vesicle, focal wall thickening of the seminal vesicle, expanded T2w hypointense ejaculatory ducts, and obliteration of the angle between prostate and seminal vesicle. Criteria for ECE included an irregular bulge in capsule, obliteration of the rectoprostatic angle, asymmetry of the neurovascular bundle, focal capsular retraction or thickening, broad capsular tumor contact (>10 mm), and direct extension of the tumor beyond the capsule. Information added from PET mainly consists of ^{68}Ga-PSMA-11 uptake of the seminal vesicles.

Clinical Staging and Risk Classification

Local tumor staging was performed by digital rectal examination. The pathologic report of the prostate biopsy was used to assess the initial Gleason grade, the number of biopsy cores taken, and the number of cores with proven PC in each individual. Clinical staging and risk classification was independent of ^{68}Ga-PSMA-11 PET/MRI.

To predict the probability of LNM as well as the local clinical stage including ECE and SVI, the Memorial Sloan Kettering Cancer Center (MSKCC) nomogram and Partin tables were used (*5*). These nomograms include the initial PSA value at diagnosis, clinical stage by digital rectal examination, the biopsy Gleason score, and the proportion of PC-affected biopsy cores. Established online calculators were used for calculating the respective scores (MSKCC nomogram: https://www.mskcc.org/nomograms/prostate/preop; Partin tables: http://urology.jhu.edu/prostate/partin_tables.php).

Surgical Procedures and Histologic Examination

All evaluated patients underwent retropubic RP including bilateral standardized pelvic lymph node dissection. RP was performed a median of 16 d (IQR, 11–27) after imaging. The resected pathologic specimens were formalin-fixed and classified according to the Union international contre le cancer, version 2002, by experienced uropathologists (*20*). Pathologic routine staging included local tumor extension, lymph node involvement, and Gleason score. The histopathologic analyses were performed with the uropathologists masked to imaging results.

Statistical Analysis

The predicted risk for LNM, ECE, and SVI was assessed for each individual patient using nomograms. The discriminatory ability of predicted probabilities for LNM, ECE, and SVI derived from nomograms was evaluated by receiver-operating-characteristic (ROC) curves. ^{68}Ga-PSMA-11 PET/MRI results for N stage were dichotomized into positive (score 1) versus negative (score 2 or 3). Areas under the curves (AUC) are presented with 95% confidence intervals (CIs) and were compared with a fixed value of 0.5. Differences between curves were assessed using DeLong's test for correlated ROC curves. Finally, ROC analyses were used for a study cohort–adjusted retrospective threshold determination for each nomogram using the Youden index. Finally, Logistic regression models including the MSKCC nomogram and ^{68}Ga-PSMA-11 PET/MRI as independent variables and histologic results as dependent variable were fitted to the data to evaluate whether ^{68}Ga-PSMA-11 PET/MRI had an explanatory ability additional to the MSKCC nomogram. For LNM Firth's logistic regression implemented in the R library logistf was used because of quasicomplete separation. Predicted event probabilities were used in the ROC analysis to compare discriminatory ability of regression model outcomes with results from the MSKCC nomogram and ^{68}Ga-PSMA-11 PET/MRI. Bootstrapping was used to compare AUCs of nested models. Cross-classified tables were used to determine sensitivity, specificity, accuracy,

positive predictive value, and negative predictive value of ^{68}Ga-PSMA-11 PET/MRI for LNM, ECE, and SVI on a patient basis. Tests were 2-sided, with a significance level of $\alpha = 5\%$. On a patient basis, the rate of full concordance between results from each method, compared with postoperative N and T stage, was assessed. All analyses were performed using SPSS version 21 (SPSS Inc.) or R version 3.3.1 (R Foundation for Statistical Computing) with the library pROC.

RESULTS

Patient Characteristics and Histopathology

A total of 102 patients were extracted from the institution's database. Seventy-three of 102 (71.6%) underwent RP and were finally eligible for analysis. Reasons for exclusion were as follows: RP at institutions other than Klinikum Rechts der Isar ($n = 8$), external-beam radiotherapy ($n = 6$), primary systemic hormone chemotherapy due to metastatic disease after ^{68}Ga-PSMA-11 PET/MRI ($n = 7$), denial of any therapy ($n = 2$), and lost to follow-up ($n = 6$). Histopathology revealed LNM in 25 of 73 patients (34.3%), and ECE and SVI were present in 53 (72.6%) and 33 (45.2%) patients, respectively. Patient characteristics and details on histopathology are summarized in Table 1.

Imaging Findings of ^{68}Ga-PSMA-11 PET/MRI and Positivity Rates of Clinical Nomograms

For LNM, ^{68}Ga-PSMA-11 PET/MRI was positive in 15 of 73 (20.6%) patients. In 2 patients, findings of ^{68}Ga-PSMA-11 PET/MRI were equivocal. Image-based local staging of the prostate revealed organ-confined disease (≤T2c) in 12 (16.4%) and non–organ-confined disease (≥T3a) in 61 (83.6%) patients. Of those 61 patients, 26 (35.6%) patients exhibited only ECE (T3a), 33 (45.2%) patients showed additional (T3b), and 2 (2.7%) patients presented with suggestion of T4 stage in imaging. Two patients were read as M-positive with single bone metastases. Figure 1 presents an example of local staging of the prostate revealing SVI and LNM in ^{68}Ga-PSMA-11 PET/MRI.

Table 2 summarizes the predicted positivity rate for LNM, ECE, and SVI for the entire patient group using the MSKCC and the Partin nomograms as well as ^{68}Ga-PSMA-11 PET/MRI in comparison to prevalence from histopathology. The pathologic prevalence of LNM was nearly ideally predicted by the MSKCC nomogram. ^{68}Ga-PSMA-11 PET/MRI and even more Partin tables underestimated the presence of LNM on a patient basis. For ECE and SVI, MKSCC nomogram and ^{68}Ga-PSMA-11 PET/MRI performed nearly equivalent, with a slight overestimation. Partin tables again led to a clear underestimation.

Comparison of Diagnostic Value for Clinical Nomograms and Results from ^{68}Ga-PSMA-11 PET/MRI Validated by Histopathology

Table 3 summarizes the diagnostic performance of the clinical nomograms based on retrospective threshold determination and results from ^{68}Ga-PSMA-11 PET/MRI. Figure 2 shows the ROC curve analyses for the prediction of LNM, ECE, and SVI using the ^{68}Ga-PSMA-11 PET/MRI and the clinical staging nomograms validated by histopathology.

For LNM, the largest AUC (0.8; 95% CI, 0.68–0.93) was found for ^{68}Ga-PSMA-11 PET/MRI, but no statistical difference could be observed in pairwise comparisons to the MSKCC nomogram (0.77; 95% CI, 0.66–0.89; $P = 0.67$) or Partin tables (0.67; 95% CI, 0.53–0.80; $P = 0.086$). Notably, all tests demonstrated a

TABLE 1
Patient Characteristics

Characteristics	No. of patients included in analysis ($n = 73$)
Median age (y)	68 (IQR, 63–73)
Median PSA at diagnosis (ng/dL)	14.0 (IQR, 6–35)
Clinical T stage at diagnosis	
T1c	17 (23.3)
T2a	11 (15.1)
T2b	19 (26.0)
T2c	8 (11.0)
T3a	14 (19.2)
T3b	4 (5.5)
Postbiopsy Gleason sum at diagnosis (*n*)	
6	3 (4.1)
7	9 (12.3)
8	33 (45.2)
9	25 (34.3)
10	3 (4.1)
Imaging T stage	
T2c	12 (16.4)
T3a	26 (35.6)
≥T3b	35 (48.0)
Imaging N stage	
cN0	56 (76.7)
cN1	15 (20.6)
Intermediate	2 (2.7)
Imaging M stage (bone metastasis)	
cM0	71 (97.3)
cM1	2 (2.7)
Postoperative T stage	
T2a	2 (2.7)
T2b	3 (4.1)
T2c	15 (20.6)
T3a	20 (27.4)
≥T3b	33 (45.2)
Postoperative N stage	
pN0	48 (66.7)
pN1	25 (34.3)
LNs	
Total no. removed	1,902
Mean removed/patients ± SD	26.1 ± 16.9
Median	23 (IQR, 17–29)
Total no. of positive LNs	165

Data in parentheses are percentages unless otherwise indicated.
Gs = Gleason sum; LNs = lymph nodes; DRE = digital rectal examination.

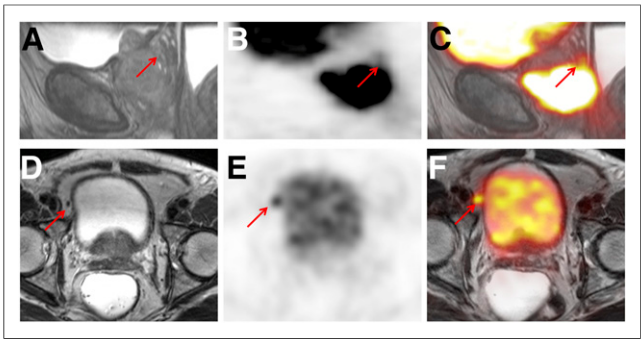

FIGURE 1. ^{68}Ga-PSMA-11 PET/MRI of a 75-y-old patient with high-risk PC. Local sagittal reformatted T2w sequence (A), PET (B), and fused PET/MRI (C) show tumorous involvement of apical two thirds of prostate, with extension into seminal vesicles (arrows). Pelvic T2w turbo spin echo (D), PET (E), and fused PET/MRI (F) demonstrate intense PSMA ligand uptake in 6-mm lymph node adjacent to bladder. Postoperative histopathology resulted in pT3b N1 stage. Variables from biopsy, PSA-value, and digital rectal examination resulted in cT3–4N1 stage for the MSKCC nomogram and cT3N0 stage for Partin tables based on thresholds from ROC analysis.

significant difference compared with a fixed level of 0.5. Notably, whereas ^{68}Ga-PSMA-11 PET/MRI and Partin tables revealed the lower sensitivities compared with the MSKCC nomogram, ^{68}Ga-PSMA-11 PET/MRI demonstrated superb specificity and positive predictive value.

For prediction of ECE, the MSKCC nomogram showed the largest AUC (0.83; 95% CI, 0.72–0.94), followed by ^{68}Ga-PSMA-11 PET/MRI (0.70; 95% CI, 0.55–0.85) although no statistical difference ($P = 0.054$) was observed. The AUC of Partin tables (0.54; 95% CI, 0.39–0.69) was not significantly different from the fixed value of 0.5 and significantly lower than the MSKCC nomogram ($P = 0.003$) but not lower than that of ^{68}Ga-PSMA-11 PET/MRI ($P = 0.11$). AUCs for the MSKCC nomogram and ^{68}Ga-PSMA-11 PET/MRI were not significantly different ($P = 0.054$). The sensitivity for detection of ECE was highest for ^{68}Ga-PSMA-11 PET/MRI at the expense of a considerably low specificity.

For prediction of SVI, AUC was highest for the MSKCC nomogram (0.88; 95% CI, 0.80–0.95), followed by ^{68}Ga-PSMA-11 PET/MRI (0.81; 95% CI, 0.70–0.91) and Partin tables (0.77; 95% CI, 0.67–0.88). No significant differences could be observed between ^{68}Ga-PSMA-11 PET/MRI and the MSKCC nomogram ($P = 0.16$) or Partin tables ($P = 0.57$). However, the AUC of the MSKCC nomogram was significantly higher than for Partin tables ($P = 0.02$). SVI was reliably detected by all tests (sensitivities > 80%), but ^{68}Ga-PSMA-11 PET/MRI revealed the highest specificity.

One-stop-shop ^{68}Ga-PSMA-11 PET/MRI, the MSKCC nomogram, and the Partin tables showed full concordance to the final histopathologic T and N stage in 44 patients (60.3%), in 38 patients (52.1%), and 29 patients (39.7%), respectively. Further comparative analyses concerning the side of tumor localization (right vs. both vs. left) in patients with concordant imaging and histologic findings of ECE or SVI ($n = 48$) revealed an accordance of 75%.

Finally, we assessed a model integrating the information from the MSKCC nomogram with ^{68}Ga-PSMA-11 PET/MRI for T and N stage. With respect to LNM, the combined use of the latter resulted in an improved AUC of 0.87 (95% CI, 0.78–0.96) versus 0.8 (95% CI, 0.68–0.93) and 0.77 (95% CI, 0.66–0.89) for ^{68}Ga-PSMA-11 PET/MRI and the MSKCC nomogram, respectively. Less improvement was found for local staging. For ECE, the merged AUC was 0.84 (95% CI, 0.72–0.95) versus 0.83 (95% CI, 0.72–0.94) for the MSKCC nomogram versus 0.70 (95% CI, 0.55–0.85) for ^{68}Ga-PSMA-11 PET/MRI, respectively. Concerning SVI, the combined information resulted in an AUC of 0.91 (95% CI, 0.84–0.97) whereas it was 0.88 (95% CI, 0.80–0.95) and 0.81 (95% CI, 0.70–0.91) for the MSKCC nomogram and ^{68}Ga-PSMA-11 PET/MRI, respectively. Thus, a statistically improved predictive value of the ^{68}Ga-PSMA-11 PET/MRI in addition to the MSKCC nomogram was found only with respect to LNM ($P = 0.01$) (Supplemental Fig. 1).

DISCUSSION

In this retrospective analysis, we investigated the value of ^{68}Ga-PSMA-11 PET/MRI for comprehensive local and nodal preoperative staging of high-risk PC compared with clinical nomograms with histopathologic validation as gold standard. To the best of our knowledge, this is the first study evaluating 1-stop-shop ^{68}Ga-PSMA-11 PET/MRI as a comprehensive 1-stop-shop whole-body imaging staging procedure for primary staging of high-risk PC patients. As a main result of the study, ^{68}Ga-PSMA-11 PET/MRI and clinical nomograms were equivalent in the determination of the clinical stage. Overall, however, a trend toward a higher accuracy of ^{68}Ga-PSMA-11 PET/MRI is evident, despite not being statistically significant. Most important, ^{68}Ga-PSMA-11 PET/MRI offers additional information on the location of tumor deposits and thus may guide surgery or radiation therapy. Notably, for our data the combination of the MSKCC nomogram as most promising clinical nomogram with the ^{68}Ga-PSMA-11 PET/MRI did translate to a considerable advantage only for the prediction of LNM.

TABLE 2
Comparison of Positivity Rate Using Clinical Nomograms, Findings in ^{68}Ga-PSMA-11 PET/MRI, and Results from Histopathology

Site	Pathologic prevalence (%)	Positivity rate (%) using clinical nomograms		Positivity rate (%) using ^{68}Ga-PSMA-11 PET/MRI
		MSKCC nomogram	Partin tables	
LNM	34.3 (25/73)	Mean ± SD, 39.7 ± 26.6; median, 32 (IQR, 19–55)	Mean ± SD, 14.1 ± 11.0; median, 10 (IQR, 7–20)	20.6 (15/73)
ECE	72.6 (53/73)	Mean ± SD, 83.6 (11.7); median, 86 (IQR, 77–93)	Mean ± SD, 38.4 (6.8); median, 40 (IQR, 36–43)	83.6 (61/73)
SVI	45.2 (33/73)	Mean ± SD, 37.6 (26.5); median, 29 (IQR, 18–54)	Mean ± SD, 19.3 (8.4); median, 20 (IQR, 13–29)	47.9 (35/73)

TABLE 3
Sensitivity, Specificity, PPV, and NPV of 1-Stop-Shop ^{68}Ga-PSMA-11 PET/MRI and Preoperative Clinical Staging Nomograms for Detection of LNM, ECE, and SVI

Site	Prediction device	Sensitivity	Specificity	PPV	NPV	AUC (95% CI)	Significance *P**	Pairwise comparison (*P*)
LNM	^{68}Ga-PSMA-11 PET/MRI	60%	100%	100%	82.8%	0.8 (0.68–0.93)	<0.001	0.67
	MSKCC nomogram, cut-off > 48.5%	68%	83.3%	68%	83.3%	0.77 (0.66–0.89)	<0.001	0.86
	Partin tables, cut-off > 19%	60%	75%	55.6%	78.2%	0.67 (0.53–0.80)	0.022	
ECE	^{68}Ga-PSMA-11 PET/MRI	94.3%	45%	82.0%	75%	0.70 (0.55–0.85)	0.01	0.054
	MSKCC nomogram, cut-off > 84.5%	66%	85%	92.1%	48.5%	0.83 (0.72–0.94)	<0.001	0.11
	Partin tables, cut-off > 37.5%	71.1%	45%	77.7%	37.5%	0.54 (0.39–0.69)	0.59	
SVI	^{68}Ga-PSMA-11 PET/MRI	81.8%	80%	77.1%	84.2%	0.81 (0.70–0.91)	<0.001	0.16
	MSKCC nomogram, cut-off > 27.5%	87.9%	75%	74.3%	88.3%	0.87 (0.80–0.95)	<0.001	0.57
	Partin tables, cut-off > 15.5%	90.9%	57.5%	63.8%	88.5%	0.77 (0.67−0.88)	<0.001	

*Significance compared with a fixed level of 0.5.
LNM: ^{68}Ga-PSMA-11 PET/MRI to MSKCC nomogram: $P = 0.67$; ^{68}Ga-PSMA-11 PET/MRI to Partin tables: $P = 0.86$.
ECE: ^{68}Ga-PSMA-11 PET/MRI to MSKCC nomogram: $P = 0.054$; ^{68}Ga-PSMA-11 PET/MRI to Partin tables: $P = 0.11$.
SVI: ^{68}Ga-PSMA-11 PET/MRI to MSKCC nomogram: $P = 0.16$; ^{68}Ga-PSMA-11 PET/MRI to Partin tables: $P = 0.57$.
PPV = positive predictive value; NPV = negative predictive value.

Until recently, imaging was regarded as inadequate for accurate preoperative staging (e.g., LNM) of high-risk PC (*2,7,11,21*). Despite MRI or CT being recommended in guidelines, the use of clinical nomograms is determinant to especially assess the risk of local advanced tumor and LNM (*1,2*). The advent of PSMA ligand PET imaging seems to enhance detection of even small PC tumor deposits substantially (*12,13,16,22–24*). Its use within a PET/MRI examination holds promise to combine superb anatomic with functional information in a 1-stop-shop procedure.

First, in our analysis on a cohort basis the risk for LNM was most closely predicted using the MSKCC nomogram (39.7%). Whereas the Partin table performed worst (14.1%), ^{68}Ga-PSMA-11 PET/MRI predicted LNM in 20.6% of patients compared with a pathologic prevalence (34.3%) (Table 3). The latter translates well into a sensitivity of approximately 60%, which is known from previous studies and a recent metaanalysis (pooled sensitivity, 61%) (*13,16,22*). However, on the basis of superb specificity on a patient basis, diagnostic performance of ^{68}Ga-PSMA-11 PET/MRI as expressed by AUC (0.8) was highest among all tests. No statistical difference was present compared with the MSKCC nomogram (0.77) and Partin tables (0.67).

In our study, the performances of the MSKCC nomogram and Partin tables were comparable to literature. The MSKCC nomogram showed an AUC of 0.77 similar to the literature (0.78) in a recent meta-analysis (*25*). With an AUC of 0.67 in our analysis, the updated Partin tables were slightly less accurate than the AUCs in prior cohorts (0.77 and 0.80) (*25–27*). The reduced accuracy might be a result of our patient cohort including only high-risk patients, as Partin tables are most powerful in low- and intermediate-risk PC (*5,26*).

Second, for assessment of ECE and SVI, our data underline that in addition to advances for intraprostatic tumor localization, ^{68}Ga-PSMA-11 PET/MRI can also aid in T staging (*12*). On a cohort basis for ECE, evaluation of ^{68}Ga-PSMA-11 PET/MRI mainly based on the multiparametric MRI data exhibited superb sensitivity with moderate specificity. This is in contrast to literature and might be related to reader experience and the combined reading of multiparametric MRI supplemented by ^{68}Ga-PSMA-11 PET (*28*). The MSKCC nomogram had moderate sensitivity but higher specificity, whereas Partin tables clearly underestimated the risk of ECE.

For SVI on a cohort basis prediction, ^{68}Ga-PSMA-11 PET/MRI was nearly perfect. Although the MSKCC nomogram and Partin tables underestimated the observed prevalence of SVI on a cohort basis, patient-based AUCs were not significantly lower than ^{68}Ga-PSMA-11 PET/MRI. The latter exhibited both fair sensitivity and specificity, whereas MSKCC nomogram and Partin tables offered slightly higher sensitivity but lower specificity. Our data for ECE and SVI using Partin tables are well comparable to a recent cohort reporting AUCs of 0.60 and 0.73, respectively (*26*).

Finally, the assessment of each staging test exhibited the highest rate of full concordance between the final histopathologic T and N stage for ^{68}Ga-PSMA-11 PET/MRI (60.3%) compared with the MSKCC nomogram (52.1%) and Partin tables (39.7%). Despite the fact that the difference especially toward the MSKCC nomogram is not exceedingly high, ^{68}Ga-PSMA-11 PET/MRI adds additional value by providing anatomic data to guide treatment (*8*). Hereby, imaging by ^{68}Ga-PSMA-11 PET/MRI offers highly specific information on the exact localization of the LNM. This is important because

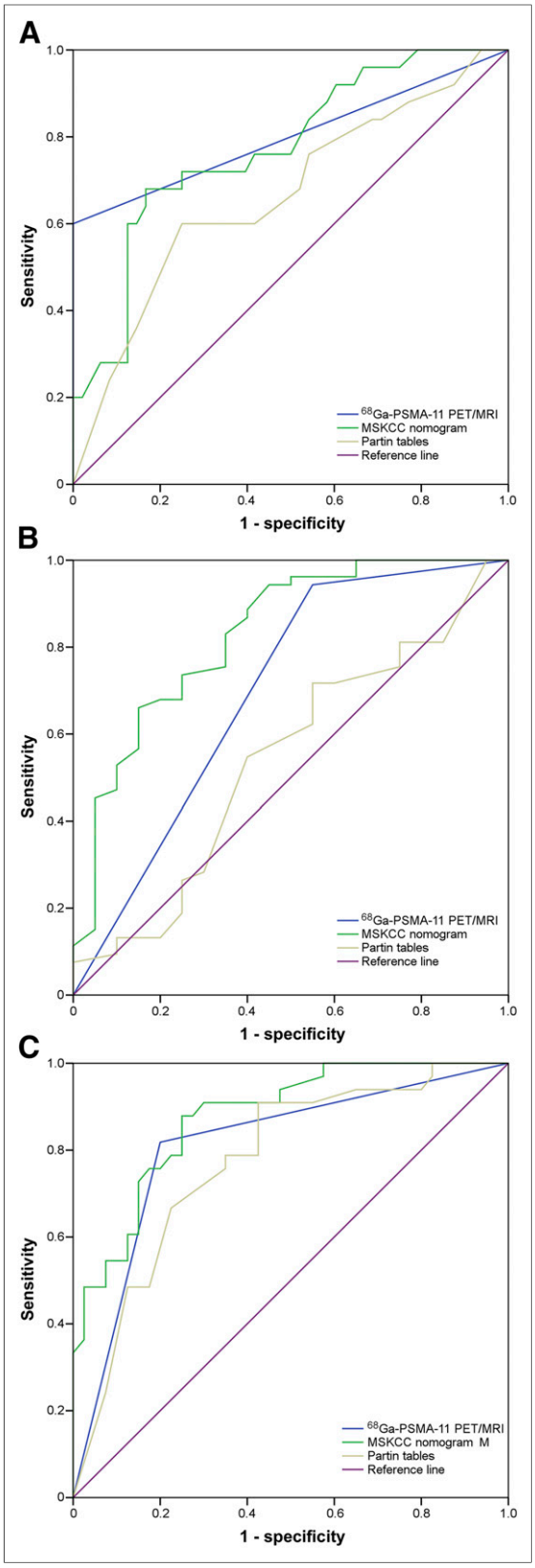

FIGURE 2. ROC curves for simultaneous ^{68}Ga-PSMA-11 PET/MRI and preoperative clinical staging nomograms for detection of LNM (A), ECE (B), and SVI (C).

appropriate lymph node staging revealed a considerable rate of LNM outside the standard pelvic lymph node dissection templates, and studies investigating specific radiolabeled LNM dissection revealed improved detection of LNM with promising biochemical response rates and progression-free survival, thus pointing out the importance of accurate staging and individualized lymphadenectomy (*29–33*). Similarly, ^{68}Ga-PSMA PET significantly influenced radiation planning due to enhanced detection of LNM (*34,35*).

Nevertheless, a considerable percentage of LNM is missed by ^{68}Ga-PSMA-11 PET that also depends on size of tumor deposits within the lymph node (especially $<$ 5 mm) (*36*). In addition, imaging in contrast to staging nomograms can tailor local resection at the site of ECE or SVI. Notably, both the MSKCC nomogram and the Partin table do not differ between cT3a and cT3b or even between cT3 and cT4 in certain risk constellations compared with ^{68}Ga-PSMA-11 PET/MRI, which offers a clear specific T stage. Nevertheless, impact on patient outcomes after image-guided primary RP or radiation therapy based on ^{68}Ga-PSMA-11 PET/MRI has to be evaluated in further prospective studies.

Our study has some limitations. First, nomograms provide a continuous risk probability and do not include a binary decision mandatory for direct comparisons of sensitivity and specificity to ^{68}Ga-PSMA-11 PET/MRI. Thus, in our study, we retrospectively used the Youden index to implement thresholds for the used nomograms. This approach is not uncommon; however, it might lead to an overestimation of the performance of nomograms as has been published previously (*7*). Second, there are potentially other nomograms for preoperative use in primary PC (e.g., Briganti nomogram, Roach formula). As these nomograms only predict N stage and do not offer prediction of T stage, we decided to omit them because they cannot be used for comprehensive preoperative staging in comparison to ^{68}Ga-PSMA-11 PET/MRI. A further potential drawback is the lack of a consensus read of the ^{68}Ga-PSMA-11 PET/MRI. However, image analysis was performed by 1 experienced double-board-certified physician and also histopathologic results were retrospectively taken from the standardized patients' records and were not uniformly reread by an uropathologist for this study. Finally, it has to be pointed out that on the basis of the spatial resolution of PET, the diagnosis of SVI and ECE within a ^{68}Ga-PSMA-11 PET/MRI is mainly based on the results from MRI. Therefore, a potential alternative (which is clinical practice in many institutions due to the lack of a PET/MR) would be to combine a ^{68}Ga-PSMA-11 PET/CT for N and M staging with a multiparametric MR for T2 staging.

CONCLUSION

Our data indicate that 1-stop-shop ^{68}Ga-PSMA-11 PET/MRI performs equally well to established clinical nomograms for preoperative staging of high-risk PC patients. It shows a trend toward a higher prediction of the comprehensive final pT and pN stage on a patient basis, although no statistical difference for comparison of results for LNM, ECE, and SVI with the MSKCC nomogram and Partin tables are observable. However, ^{68}Ga-PSMA-11 PET/MRI yields additional information on the anatomic location of tumor deposits and thus might enable targeted treatment. In clinical routine, ^{68}Ga-PSMA-11 PET/MRI as 1-stop-shop imaging investigation might support treatment planning that may lead to enhanced oncologic results. This hypothesis has to be evaluated in further studies.

DISCLOSURE

No other potential conflict of interest relevant to this article was reported.

ACKNOWLEDGMENTS

We thank the Institute for Medical Statistics, Technische Universität München, Germany, for counseling.

REFERENCES

1. Mohler JL, Armstrong AJ, Bahnson RR, et al. Prostate cancer, version 1. *J Natl Compr Canc Netw.* 2016;14:19–30.
2. Mottet N, Bellmunt J, Bolla M, et al. EAU-ESTRO-SIOG guidelines on prostate cancer. part 1: screening, diagnosis, and local treatment with curative intent. *Eur Urol.* 2017;71:618–629.
3. D'Amico AV, Whittington R, Malkowicz SB, et al. Biochemical outcome after radical prostatectomy, external beam radiation therapy, or interstitial radiation therapy for clinically localized prostate cancer. *JAMA.* 1998;280:969–974.
4. Briganti A, Larcher A, Abdollah F, et al. Updated nomogram predicting lymph node invasion in patients with prostate cancer undergoing extended pelvic lymph node dissection: the essential importance of percentage of positive cores. *Eur Urol.* 2012;61:480–487.
5. Eifler JB, Feng Z, Lin BM, et al. An updated prostate cancer staging nomogram (Partin tables) based on cases from 2006 to 2011. *BJU Int.* 2013;111:22–29.
6. Roach M, 3rd, Marquez C, Yuo HS, et al. Predicting the risk of lymph node involvement using the pre-treatment prostate specific antigen and Gleason score in men with clinically localized prostate cancer. *Int J Radiat Oncol Biol Phys.* 1994;28:33–37.
7. Schiavina R, Scattoni V, Castellucci P, et al. ^{11}C-choline positron emission tomography/computerized tomography for preoperative lymph-node staging in intermediate-risk and high-risk prostate cancer: comparison with clinical staging nomograms. *Eur Urol.* 2008;54:392–401.
8. Wang L, Hricak H, Kattan MW, Chen HN, Scardino PT, Kuroiwa K. Prediction of organ-confined prostate cancer: incremental value of MR imaging and MR spectroscopic imaging to staging nomograms. *Radiology.* 2006;238:597–603.
9. Hövels AM, Heesakkers RA, Adang EM, et al. The diagnostic accuracy of CT and MRI in the staging of pelvic lymph nodes in patients with prostate cancer: a meta-analysis. *Clin Radiol.* 2008;63:387–395.
10. Evangelista L, Guttilla A, Zattoni F, et al. Utility of choline positron emission tomography/computed tomography for lymph node involvement identification in intermediate- to high-risk prostate cancer: a systematic literature review and meta-analysis. *Eur Urol.* 2013;63:1040–1048.
11. European Association of Urology guideline on prostate cancer. European Association of Urology website. http://uroweb.org/guideline/prostate-cancer. Accessed August 28, 2018.
12. Eiber M, Weirich G, Holzapfel K, et al. Simultaneous ^{68}Ga-PSMA HBED-CC PET/MRI improves the localization of primary prostate cancer. *Eur Urol.* 2016;70:829–836.
13. Maurer T, Gschwend JE, Rauscher I, et al. Diagnostic efficacy of ^{68}Gallium-PSMA positron emission tomography compared to conventional imaging for lymph node staging of 130 consecutive patients with intermediate to high risk prostate cancer. *J Urol.* 2016;195:1436–1443.
14. Afshar-Oromieh A, Avtzi E, Giesel FL, et al. The diagnostic value of PET/CT imaging with the ^{68}Ga-labelled PSMA ligand HBED-CC in the diagnosis of recurrent prostate cancer. *Eur J Nucl Med Mol Imaging.* 2015;42:197–209.
15. Eiber M, Maurer T, Souvatzoglou M, et al. Evaluation of hybrid ^{68}Ga-PSMA ligand PET/CT in 248 patients with biochemical recurrence after radical prostatectomy. *J Nucl Med.* 2015;56:668–674.
16. Eiber M, Fendler WP, Rowe SP, et al. Prostate-specific membrane antigen ligands for imaging and therapy. *J Nucl Med.* 2017;58(suppl 2):67S–76S.
17. Li R, Ravizzini GC, Gorin MA, et al. The use of PET/CT in prostate cancer. *Prostate Cancer Prostatic Dis.* 2018;21:4–21.
18. Eder M, Neels O, Muller M, et al. Novel preclinical and radiopharmaceutical aspects of [^{68}Ga]Ga-PSMA-HBED-CC: a new PET tracer for imaging of prostate cancer. *Pharmaceuticals (Basel).* 2014;7:779–796.
19. Likert R. A technique for the measurement of attitudes. *Arch Psychol.* 1932; 22:1–55.
20. Sobin LH, Wittekind C, eds. Urological tumours: prostate. In: *TNM Classification of Malignant Tumours.* 6th ed. New York, NY: Wiley-Liss; 2002:184–188.
21. Budiharto T, Joniau S, Lerut E, et al. Prospective evaluation of ^{11}C-choline positron emission tomography/computed tomography and diffusion-weighted magnetic resonance imaging for the nodal staging of prostate cancer with a high risk of lymph node metastases. *Eur Urol.* 2011;60:125–130.
22. von Eyben FE, Picchio M, von Eyben R, Rhee H, Bauman G. ^{68}Ga-labeled prostate-specific membrane antigen ligand positron emission tomography/computed tomography for prostate cancer: a systematic review and meta-analysis. *Eur Urol Focus.* November 15, 2016 [Epub ahead of print].
23. Maurer T, Eiber M, Schwaiger M, Gschwend JE. Current use of PSMA-PET in prostate cancer management. *Nat Rev Urol.* 2016;13:226–235.
24. James N, Graham J, Maurer T, Eiber M, Gschwend JE. Diagnosis and treatment of prostate cancer: what Americans can learn from international oncologists. *Am Soc Clin Oncol Educ Book.* 2017;37:344–357.
25. Cimino S, Reale G, Castelli T, et al. Comparison between Briganti, Partin and MSKCC tools in predicting positive lymph nodes in prostate cancer: a systematic review and meta-analysis. *Scand J Urol.* 2017;51:345–350.
26. Leyh-Bannurah SR, Gazdovich S, Budäus L, et al. Population-based external validation of the updated 2012 Partin tables in contemporary north American prostate cancer patients. *Prostate.* 2017;77:105–113.
27. Abdollah F, Cozzarini C, Sun M, et al. Assessing the most accurate formula to predict the risk of lymph node metastases from prostate cancer in contemporary patients treated with radical prostatectomy and extended pelvic lymph node dissection. *Radiother Oncol.* 2013;109:211–216.
28. de Rooij M, Hamoen EH, Witjes JA, Barentsz JO, Rovers MM. Accuracy of magnetic resonance imaging for local staging of prostate cancer: a diagnostic meta-analysis. *Eur Urol.* 2016;70:233–245.
29. Heck MM, Retz M, Bandur M, et al. Topography of lymph node metastases in prostate cancer patients undergoing radical prostatectomy and extended lymphadenectomy: results of a combined molecular and histopathologic mapping study. *Eur Urol.* 2014;66:222–229.
30. Suardi N, Gandaglia G, Gallina A, et al. Long-term outcomes of salvage lymph node dissection for clinically recurrent prostate cancer: results of a single-institution series with a minimum follow-up of 5 years. *Eur Urol.* 2015;67:299–309.
31. Abdollah F, Briganti A, Montorsi F, et al. Contemporary role of salvage lymphadenectomy in patients with recurrence following radical prostatectomy. *Eur Urol.* 2015;67:839–849.
32. Maurer T, Gschwend JE, Eiber M. Prostate-specific membrane antigen-guided salvage lymph node dissection in recurrent prostate cancer: a novel technology to detect lymph node metastases. *Curr Opin Urol.* 2018;28:191–196.
33. Rauscher I, Düwel C, Wirtz M, et al. Value of ^{111}In-prostate-specific membrane antigen (PSMA)-radioguided surgery for salvage lymphadenectomy in recurrent prostate cancer: correlation with histopathology and clinical follow-up. *BJU Int.* 2017;120:40–47.
34. Dewes S, Schiller K, Sauter K, et al. Integration of ^{68}Ga-PSMA-PET imaging in planning of primary definitive radiotherapy in prostate cancer: a retrospective study. *Radiat Oncol.* 2016;11:73.
35. Schiller K, Sauter K, Dewes S, et al. Patterns of failure after radical prostatectomy in prostate cancer - implications for radiation therapy planning after ^{68}Ga-PSMA-PET imaging. *Eur J Nucl Med Mol Imaging.* 2017;44:1656–1662.
36. Jilg CA, Drendel V, Rischke HC, et al. Diagnostic accuracy of Ga-68-HBED-CC-PSMA-ligand-PET/CT before salvage lymph node dissection for recurrent prostate cancer. *Theranostics.* 2017;7:1770–1780.